Contents lists available at ScienceDirect

Electrochimica Acta

journal homepage: www.elsevier.com

Electrochemical films deposition and electro-optical properties of bis-carbazol-triphenylamine end-caped dendrimeric polymers

María I. Mangione[a, **], Rolando A. Spanevello[a], Daniela Minudri[b], Pablo Cavallo[b], Luis Otero[b], Fernando Fungo[b, *]

[a] Instituto de Química Rosario, Facultad de Ciencias Bioquímicas y Farmacéuticas, Universidad Nacional de Rosario-CONICET, Suipacha 531, S2002RLK Rosario, Argentina
[b] Departamento de Química, Universidad Nacional de Río Cuarto, Agencia Postal N° 3, X5804BYA, Río Cuarto, Argentina

ARTICLE INFO

Article history:
Received 9 October 2017
Received in revised form 19 December 2017
Accepted 20 December 2017
Available online xxx

Keywords:
Dendrimeric polymers
Electrodeposition
Optoelectronic

ABSTRACT

A family of structurally related π-conjugated star-shape bis-carbazol-triphenylamine end-caped dendrimers was designed, synthetized and characterized as novel organic optoelectronic materials. These compounds hold triphenylamine and carbazole electroactive moieties as dendrimer core and/or periphery groups. Homogeneous and stable electrogenerated polymeric films were obtained from dendrimers over Pt and ITO electrodes. These films showed charge conductivities, reversible electrochemical behavior and electrochromic effect. The hole mobility of the electrodeposited films was found to be dependent of the dendrimeric structure and film morphologies, indicating that the shape and size of the studied dendrimers have a strong effect on their charge transport properties. These results provide data that will contribute to the systematic study for the design of new dendrimers as starting materials for conductive polymers films with potential applications in optoelectronic devices.

1. Introduction

Organic materials are gaining a marked increase in their applications in electronics and optoelectronic devices, like field effect transistors [1], solar cells [2], light emitting diodes [3], and electrochromic windows [4]. However, the development of new organic materials for their use in electronic or optoelectronic systems is usually a complex challenge. The organic compounds must be designed and synthesized having molecular structures that confers a series of special characteristics to the materials that would allow them to be used as building blocks in high efficient devices [5]. These characteristics often include light absorption-emission efficiencies, appropriate electron-hole mobility, correct work function alignment, thin film formation capability, mechanical and chemical stabilities. Recently we developed series of dendrimeric materials whose molecular structures allowed the formation of polymeric films by electrochemical synthesis with charge transport and electrochromic capabilities [6–8]. Dendrimers are molecules with a three-dimensional architecture that holds multiple branches emanating from a single core [9]. They present well-defined structures, high monodispersity, and can be accurately designed containing discrete functionalities in order to obtain multifunctional materials. Dendrimers have found promising applications as constituent materials in organic electronic devices, such as transistors [10], solar cells [10], and OLEDs [11,12]. This is due to the fact that some specific dendrimeric molecules exhibit low energy barrier for hole injection, electron injection blocking capability, and good charge transporting properties [5,13]. It is also relevant the high glass-transition temperature usually shown by starburst molecules, which precludes the degradation processes due to morphological changes originated by warming during the device operation [14–16].

On the other hand, film formation and deposition methodology play key roles for the application of organic polymers in the construction of electronic devices at industrial scale production [17,18]. Thermal evaporation and/or solution-processing methods are traditionally used in the laboratory research, although they are often difficult and expensive for industrial production [19]. Thermal evaporation requires materials with adequate sublimation capability and thermal stability. Solution processes (spin or dip-coating) require organic polymeric materials with inherent high solubility, which is hard to obtain with polymers. Both methods usually produce large amounts of waste. In contrast, the electrochemical polymerization over different substrates of electroactive monomers allows the simultaneous synthesis and deposition of the polymeric film, with easy and adequate control on film thickness [20,21]. Its implementation at industrial scale is usually simple and cost effective [19]. Moreover, the polymeric films electrochemically generated over conductive substrates are usually stable, and possess adequate electrical contact with the base material. In this sense, we have demonstrated that it is possible to optimize the polymer optoelectronic properties [7,9,22–25] by manipulating the electrochemical deposition parameters. We have previously mentioned, the electrosynthesis and characterization of conductive polymers from triphenylamine (TPA) [7,17] and carbazole (CBZ) [6,26] end-capped dendrimers. The structures contained TPA moieties as core, behaved as conductive dendrimeric polymers that can be reversible charged, both at the core and the peripheral units. The electrosynthesized layers hold electrical conductivity, undergo reversible electrochemical processes and possess suitable chemical stability. We have demonstrated that star-shape dendrimers are able to form electrochemically active hyperbranched

* Corresponding author.
** Corresponding author.
Email addresses: mangione@iquir-conicet.gov.ar (M.I. Mangione); ffungo@exa.unrc.edu.ar (F. Fungo)

https://doi.org/10.1016/j.electacta.2017.12.137
0013-4686/

macromolecules with potential applications in electronic and opto-electronic devices. We have also established relationships between the molecular structural parameters and the electro-optical properties in the thin films.

Herein we report the synthesis and electrochemical characterization of a series of structural related fully conjugated dendrimeric molecules holding 4,4′-di (carbazol-9-yl)-4″-**R**-triphenylamine end-capping dendrimers, where **R** denotes the conjugated chain that binds this peripheral group to the dendrimeric core (Fig. 1).

These dendrimers possess at the end of each branch two electropolimerizable CBZ units linked to an electroactive TPA residue; a molecular scaffold closely related to 4,4′,4″-tris(N-carbazolyl)-triphenylamine (TCTA), which is a well-known hole transport material (HTM) used in many optoelectronic applications [27,28]. The dendrimeric monomers were obtained by a convergent synthetic strategy. The starburst monomers featuring di- or tri-branched structures were generated with the presence or absence of electroactive TPA central core. The CBZ residues allow the formation of hyperbranched polymeric films over conductive substrates by electrochemical polymerization. The electro-generated layers exhibited reversible redox-activity with strong color changes upon electro-oxidation, which can be switched by potential modulation. The electrochromic capability was evaluated and the spectral changes were interpreted on the basis of spectroelectrochemical analysis. On the other hand, the charge transport properties of the electrodeposited films were studied to provide further understanding of the influence of the dendrimer structural parameters over the hole mobility capability.

2. Experimental

2.1. Synthesis

Compounds D1 and D3: Core **10** (54.0 mg, 0.058 mmol) was dissolved in anhydrous THF (3.0 mL) under inert atmosphere. $Pd(PPh_3)_2Cl_2$ (5.4 mg, 0.008 mmol), CuI (2.6 mg, 0.013 mmol) and PPh_3 (1.5 mg, 0.006 mmol) were added to this solution and the mixture was stirred for 15 min. Anhydrous triethylamine (2.0 mL) was added and the reaction was stirred for 30 min. Dendron **18** (159.8 mg, 0.228 mmol) was dissolved in anhydrous THF (8.0 mL) under argon atmosphere and added to the reaction. The resulting bright yellow solution was stirred at room temperature for 2 days. Solutions were concentrated under reduced pressure and the residue was purified by flash chromatography (hexane/dichloromethane) affording two fractions: **D1** (less polar) 29.1 mg (0.021 mmol, 36%) as yellow solid and **D3** (more polar) 72.3 mg (0.027 mmol, 30%) as orange solid; **D1**: mp (dichloromethane:hexane) 180–182 °C, yellow solid; FT-IR (KBr, cm^{-1}): 3041, 2198 (C≡C), 1506, 1448, 1308, 1227, 830, 746, 721; ^1H NMR: δ (300 MHz, $CDCl_3$, TMS): 8.17 (d, J = 7.7 Hz, 8H), 7.56–7.41 (m, 44H), 7.38–7.29 (m, 12H), 7.17 (d, J 16.3 Hz, 2H), 7.05 (d, J 16.0 Hz, 2H); ^{13}C NMR: δ (75 MHz, $CDCl_3$): 147.1, 146.3, 141.0, 138.4, 137.7, 132.9, 132.6, 132.3, 129.5, 128.1, 128.0, 126.8, 126.4, 125.9, 125.2, 123.3, 120.3, 119.9, 109.8, 82.4, 75.0. MALDI-TOF MS: calcd for $C_{104}H_{69}N_6^+$, (MH^+) m/e 1401.56, found: m/e 1401.57. **D3**: mp: 188–190 °C (dichloromethane:hexane); FR-IR (KBr, cm^{-1}): 3040, 1591, 1506, 1450, 1310, 1227, 1180, 830, 748, 723; ^1H NMR: δ (300 MHz, $CDCl_3$, TMS): 8.17 (d, J 7.7 Hz, 12H), 7.75–7.38 (m, 86H), 7.36–7.28 (m, 18H), 7.18–7.09 (m, 8H), 7.11 (d, J 15.0 Hz,

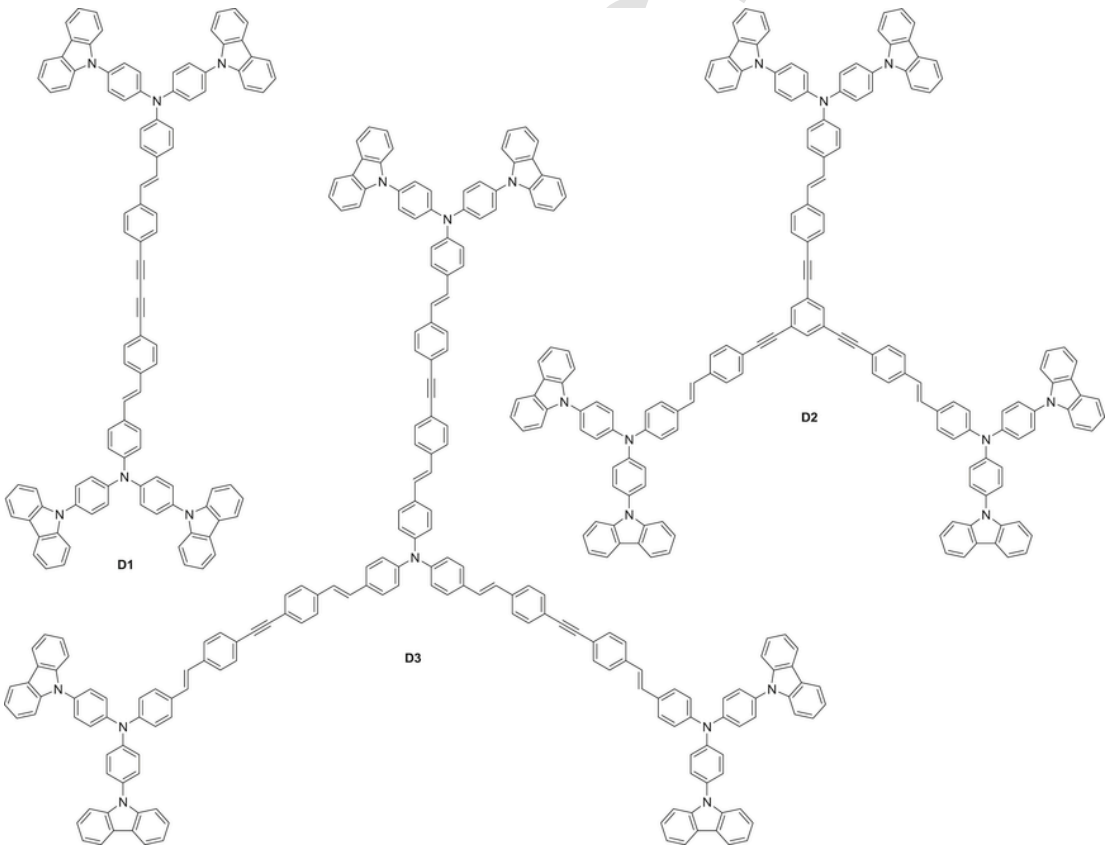

Fig. 1. Structures of analyzed compounds **D1**, **D2** and **D3**.

4H), 7.07 (d, J 15.7 Hz, 4H); ^{13}C NMR: δ (75 MHz, $CDCl_3$, TMS): 146.9, 146.8, 146.4, 141.0, 137.7, 137.5, 137.4, 132.9, 132.6, 132.1, 131.9, 128.9, 128.8, 128.1, 127.9, 127.6127.1, 126.8, 126.4, 126.3, 125.9, 125.2, 124.7, 124.3, 123.3, 122.2, 122.0, 120.4, 119.9, 109.8, 90.7, 90.6. MALDI-TOF MS: calcd for $C_{198}H_{133}N_{10}^{+}$, (MH^+) m/e 2650.07, found: m/e 2650.42.

Compound D2: Dendron **15** (100.0 mg, 0.124 mmol) was dissolved in a mixture of anhydrous trimethylamine: toluene (1:1, 10 mL). $Pd(PPh_3)_4$ (8.0 mg, 0.007 mmol) and CuI (3.9 mg, 0.020 mmol) were added and the mixture was stirred for 15 min at room temperature. Core **6** (4.8 mg, 0.032 mmol) was added to the reaction and the resulting mixture was stirred at 75 °C for two days. Solutions were concentrated under reduced pressure and the residue was purified by flash chromatography (hexane/dichloromethane) yielding **D2** (28.0 mg, 0.013 mmol, 40%) as orange solid; mp: 198–200 °C (dichloromethane:hexane); FT-IR (KBr, cm^{-1}): 3042, 2367, 1506, 1448, 1308, 1227, 1179, 1015, 830, 746, 721; ^{1}H NMR, δ (300 MHz, $CDCl_3$, TMS): 8.15 (d, J 7.8 Hz, 12H), 7.66 (s, 3H), 7.53–7.40 (m, 66H), 7.32–7.27 (m, 18H), 7.15 (d, J 16.2 Hz, 3H), 7.04 (d, J 16.2 Hz, 3H); ^{13}C NMR, δ (75 MHz, $CDCl_3$, TMS): 147.0, 146.3, 142.0, 137.8, 134.0, 132.6, 132.5, 132.1, 129.1, 128.1, 128.0, 127.0, 126.4, 126.0, 125.2, 124.6, 124.2, 123.4, 121.6, 120.4, 119.9, 109.8, 90.0, 88.8. MALDI−TOF (m/e): calcd for $C_{162}H_{105}N_9$, 2175.85 (M+); obsd. 2175.52.

2.2. Instrumentation and characterization techniques

Melting points were taken on a Leitz Wetzlar Microscope Heating Stage, Model 350 apparatus and are uncorrected. 1H and 13C NMR spectra were recorded on Bruker Avance-300 spectrometer with Me4Si as the internal standard and chloroform-d as solvent. Abbreviations: s = singlet, d = doublet, t = triplet, and m = multiplet expected but not resolved. Mass spectra of dendrons were recorded in a Shimadzu QP2010 Plus instrument, ion source temperature = 300 °C, and detector voltage = 70 kV. Samples were analyzed by ultraviolet matrix assisted laser desorption-ionization mass spectrometry (UV−MALDIMS) and by ultraviolet laser desorption-ionization mass spectrometry (UV−LDI MS) performed on a Bruker Ultraflex Daltonics TOF/TOF mass spectrometer Mass spectra were acquired in linear positive and negative ion modes. Stock solutions of samples were prepared in chloroform. External mass calibration was made using β-cyclodextrin (MW 1134) with nHo as matrix in positive and negative ion mode. Sample solutions were spotted on a MTP 384 target plate polished steel from Bruker Daltonics (Leipzig, Germany). For UV−MALDI MS matrix solution was prepared by dissolving GA (gentisic acid, 1 mg/mL) in water and dry droplet sample preparation was used according to Nonami et al. [29] loading successively 0.5 μL of matrix solution, analyte solution and matrix solution after drying each layer at normal atmosphere and room temperature. For UV-LDI MS experiments two portions of analyte solution (0.5 μL × 2) were loaded on the probe and dried successively (two dry layers). Desorption/Ionization was obtained by using the frequency-tripled Nd:YAG laser (355-nm). The laser power was adjusted to obtain high signal-to-noise ratio (S/N) while ensuring minimal fragmentation of the parent ions and each mass spectrum was generated by averaging 100 lasers pulses per spot. Spectra were obtained and analyzed with the programs FlexControl and FlexAnalysis, respectively. Reactions were monitored by TLC on 0.25 mm E. Merck Silica Gel Plates (60F254), using UV light (254 nm) and phosphomolybdic acid as developing agent. Flash column chromatographies using E. Merck silica gel 60H were performed by gradient elution of mixture of n-hexane and increasing volumes of dichloromethane or ethyl acetate. Reactions were run under an argon atmosphere with freshly distilled anhydrous solvents, unless otherwise noted. Yields refer to chromatographically and spectroscopically homogeneous materials, unless otherwise stated.

Optical Characterization: Shimadzu UV-2401PC spectrometer and Spex FluoroMax fluorometer were used to obtain the absorption and fluorescence spectra, respectively. Spectra were recorded using quartz cells (path length: 1 cm) at room temperature.

Electrochemical Study and Polymer Films Electrodeposition: Electrochemical measurements were performed at room temperature with a CHI6208E electrochemical analyzer. The dendrimers concentrations were in the 0.5–1.0 mM range in 1,2- dichloroethane (DCE) solution containing 0.1 M tetra-*n*-butylammonium hexafluorphosphate (TBAHFP) as support electrolyte. Cyclic voltammetry was conducted in a three-electrode cell with an inlaid platinum disk (2.16×10^{-3} cm^2) as a working electrode, which was polished on a felt pad with 0.3 μm alumina. A platinum wire was used as an auxiliary electrode. All cell potentials were taken with the use of a silver wire as pseudoreference electrode. All potential values in this study are expressed relative to a ferrocene/ferrocenium redox couple (Fc/Fc^+ = 0.40 V vs SCE) that was added to the solution as an internal standard [30]. A solvent−electrolyte blank experiment was performed to discard possible active electrochemically interferes prior to perform the electrochemical studies on the dendrimers solutions.

Spectroelectrochemical: The dendrimeric electrodeposited films spectroelectrochemical and electrochromic properties were studied by a CHI6208E electrochemical analyzer along with an Agilent HP 8453 UV–Visible diode-array spectrophotometer. These experiments were carried out in a homemade cell built from a commercial UV–visible cuvette (See photograph showed in Fig. 5). The films were electropolymerized on ITO (indium tin oxide, Delta Technologies, nominal resistance 10 Ω/sq, 50 mm × 7 mm × 0.9 mm) electrodes by cyclic voltammetry method under the experimental conditions described above. The background correction was made by taking a blank of the ITO working electrode without the polymer film.

Film Analysis: The films thicknesses were measured with a KLA-Tencor profilometer model AlphaStep D-600 Stylus Profiler. The surfaces of electrodeposited polymer films were analyzed by scanning electron microscopy (SEM-Carl Zeiss EVO MA 10 with electron beam energy of 18 KV).

2.3. Devices fabrication for hole mobility measurement

The polymer film was electrodeposited as hole-transporting layer (HTL) on ITO (2 mm wide band) with a resistance of 8–12 Ω/sq. The ITO band (3 × 50 mm) was etched with the traditional process of halogen acids with concentrations higher than about 6 M and metal Zn. After etching, the samples were rinsed with non-ionic detergent and deionized water, ultrasonicated in isopropanol and dried. After polymer film formation the electrodes were washed with fresh DCE to remove rest of electrolyte and dried overnight at 80 °C in a vacuum oven. Single-layer devices were built with the following configuration: ITO/dendrimeric-polymer film (variable thickness)/Ag (~250 nm). Ag contacts were thermally evaporated through the shadow mask using ULVAC (VPC-1100) equipment, obtaining four devices, with an area of 0.04 cm^2 each one. These single layer-devices were introduced into a bell jar and the I—V curves were measured at room temperature under vacuum, with a computer-controlled Keithley 2400 SourceMeter.

3. Results and discussion

3.1. Synthesis and characterization

All dendrimers (Fig. 1) were obtained by Sonogashira coupling between the cores 1,3,5-triethynylbenzene (TEB) **6** or *tris*{4-[(E)-2-

(4-iodophenyl)vinyl]phenyl}amine **10** and the corresponding dendrons with exception of **D1** which was obtained through an homocoupling process. The synthesis of cores **6** and **10** were previously described by our group and the synthetic steps are described in Scheme 1 [7].

Synthesis of carbazole-triphenylamine dendrons **15** and **18** were accomplished starting from commercial triphenylamine **7**. Vilsmeier-Haack mono-formylation of **7** afforded aldehyde **11** which was submitted to an iodination reaction yielding compound **12**. Diiodide **12** was coupled with carbazole **13** under modified Ullmann's conditions to afford **14** in 79% yields. Wadsworth-Horner-Emmons *trans*-olefination of **14** with the synthetic phosphonate **9** generates dendron **15**. Sonogashira-type coupling reaction of **15** with commercially available reagent **16** generates protected alkyne **17** with 90% of yield. Finally, **17** was deprotected under basic conditions to produce free alkyne **18** in 87% of yield. All the compounds were solids and were purified by crystallization or flash chromatography. All the synthetic steps gave very good yields (Scheme 2).

Dendrimers were obtained by coupling between core **6** and dendron **15** and core **10** with dendron **18**. **D1** was generated through the Glaser's [31] homocoupling of dendron **18**. Palladium catalysts were different for each Sonogashira's coupling. $Pd(PPh_3)_2Cl_2$ catalyst was employed for the coupling reaction between core **6** and dendron **15** (Scheme 3), while $Pd(PPh_3)_4$ was better catalyst for the cross-coupling reaction between core **10** and dendron **18** affording higher yields of **D3**. As depicted in Scheme 3 reactions showed moderated yields. All compounds with extended π-conjugation were purified by flash chromatography and crystallized producing yellow to orange solids.

The cores and dendrons structures were confirmed by ^{1}HNMR, ^{13}CNMR and FT-IR spectroscopy, and compared with the corresponding bibliographic reference when it was necessary. Structures of the compounds were also characterized by ^{1}HNMR, ^{13}CNMR, FT-IR spectroscopy and MALDI-TOF mass spectrometry experiments. In the conjugated macromolecules **D1**, **D2** and **D3** the observation of two alkyne signals and the total number of different carbon atoms signals in the ^{13}CNMR spectrum allowed us to confirm the star-shape

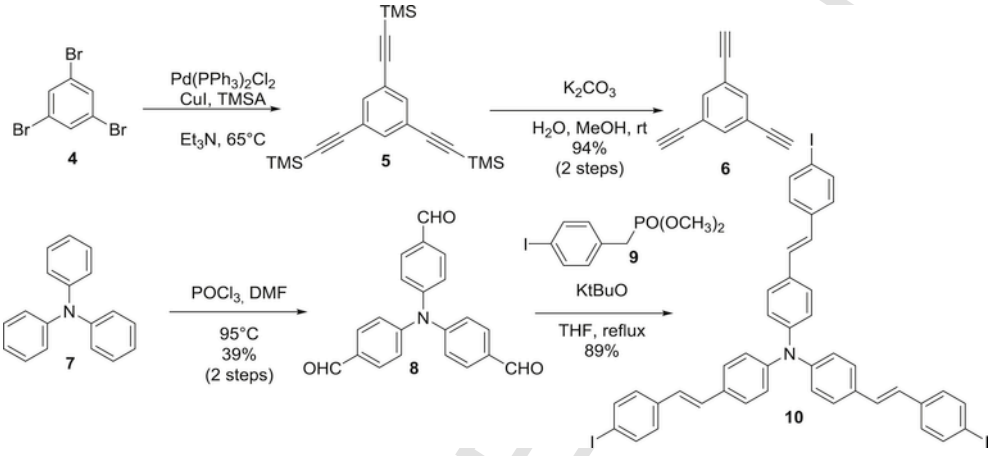

Scheme 1. Synthesis of cores **6** and **10**.

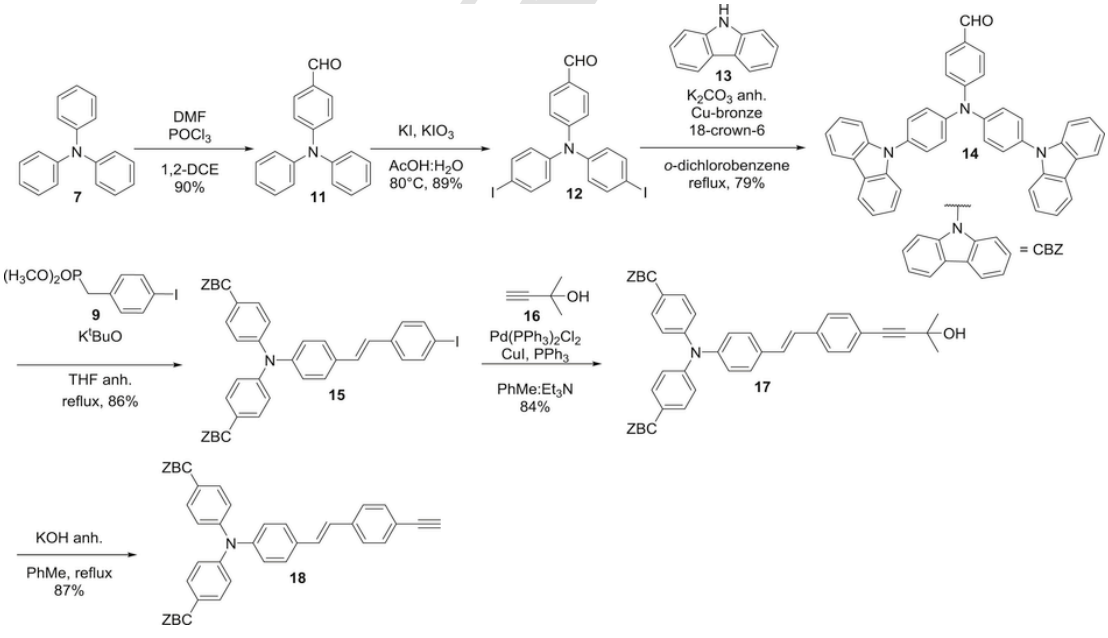

Scheme 2. Synthesis of dendrons **15** and **18**.

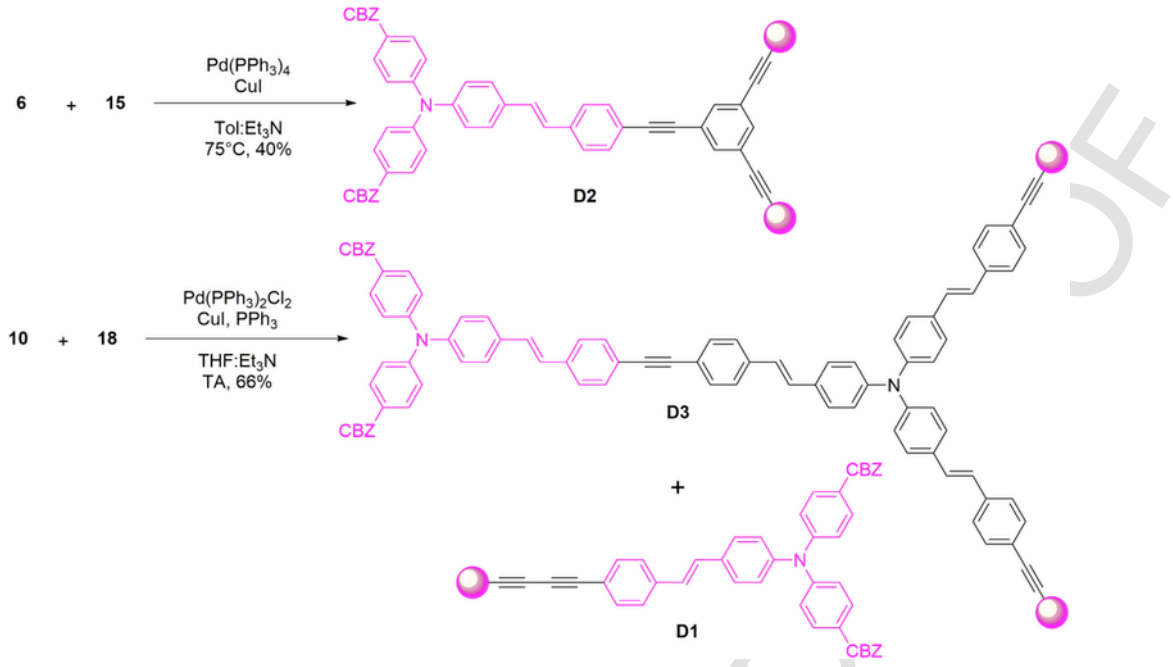

Scheme 3. Synthesis of **D1**, **D2** and **D3**.

of the **D2** and **D3** and the linear structure of **D1**. Experimental details and NMR spectra (uni- and bidimensional) are described in the Supporting Information.

3.2. Dendrimers optical properties

Fig. 2 shows the dendrimers' UV–vis s light absorption spectra for both DCE and toluene (PhMe) dilute solutions. The graphics demonstrated that the three monomers have similar optical characteristics and the electronic transitions are solvent polarity independent. The absorption spectra display two prominent bands, one in the UV region at ~330 nm, meanwhile the second appears in the 395–420 nm range. The corresponding data to the maximum absorption wavelengths are summarized in Table 1. It is expected that the optical behavior of the compounds is ruled by the different chromophores that make up the dendrimer macromolecular structures. Therefore, the absorption band that appears at 330 nm could be assigned to the TPA and CBZ centers [24,26,32], whereas the low energy band, centered

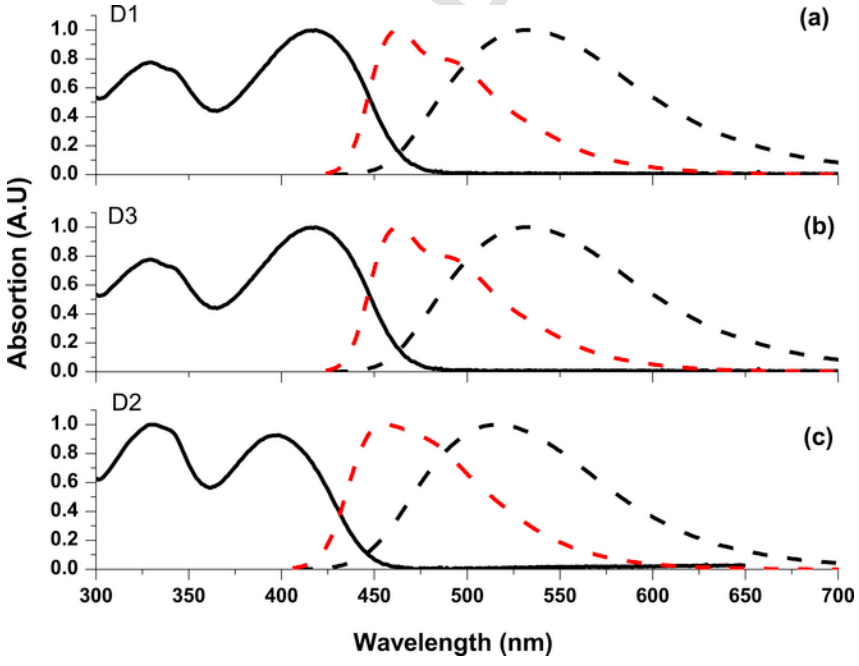

Fig. 2. Normalized light absorption (—) and emission (- - -) spectra of the dendrimers in different polarity solvents. DCE (black) and PhMe (Red). Due the similarity of the dyes absorption spectra in both solvents, it is shown in DCE. (For interpretation of the references to color in this figure legend, the reader is referred to the Web version of this article.)

Table 1
Photophysical and electrochemical parameters of the dendrimers.

	Photophysical				Electrochemical		Energy Levels[g]
	Ab. ($\lambda_{máx}$)		*Emission* ($\lambda_{máx}$)		*Oxidation Potentials* (*V*)		
	DCE[a]	λ_{film}^{onset}	DCE[a]	PhMe[a]	$E^{\#}_{\text{Monomer}}$	$E^{\#}_{\text{Film}}$	LUMO HOMO
D1	329/ 418	495[b]	532	462	0.35[c]/0.82[d]/1.19[b]	0.29[e] (210)[f]	−2.89 −5.39
D2	329/ 396	491[b]	516	456	0.44[c]/0.85[d]/1.20[b]	0.40[e] (363)[f]	−2.97 −5.50
D3	330/ 419	460[b]	520	466	0.33[c]/0.72[d]/1.22[b]	0.31[e] (180)[f]	−2.71 −5.41

[a] Absorption and emission wavelength maxima (nm) taken from UV–vis spectra of dendrimers in solution. The emission spectra were measured by excitation at the maximum wavelength of the lower energy absorption bands.

[b] Low energy optical onset of the electrodeposited films, as determined from the intersection between the projection of the corresponding spectrum in the reduced state and the base line.

[c] Reversible process-half-wave potentials.

[d] Peak potential.

[e] Onset potentials of the electrodeposited films determined from intersection between the baseline and the current signal. The potentials values are expressed in volt vs. Fc/Fc^{+}.

[f] Film thickness in nm.

[g] Calculated [30] HOMO and LUMO energies of the dendrimeric films in the absolute scale (eV) as obtained using the following equations: $HOMO = -\left(E^{\#}_{Film} + 5.1\right)(eV)$, $LUMO = HOMO + E^{Optical}_{Gap}$ and $E^{Optical}_{Gap} = 1240/\lambda^{onset}_{film}$.

around of 410 nm in the visible region, could be attributed to the π–π* transition taking place in the *p*-phenylenevinylene segment [24,26]. It is remarkable that the absorption maxima due π–π* transition in (**D1**) and (**D3**) are red shifted with respect to (**D2**). This behavior could be associated with the different conjugation lengths of the dendrons. On the other hand, the lack of solvent polarity effect in the absorption spectra indicates that the electronic states involved in the optical transitions have low charge-transfer character.

All of the dendrimers exhibit photoluminescence at room temperature when they are excited at the maximum wavelength of their low energy absorption bands. As can be observed in Fig. 2, the fluorescence spectra are solvent polarity sensitive. The dendrimer emission maximum wavelengths, unlike to the observed for light absorption, show a marked redshift (more than 50 nm) when the solvent polarity is increased from PhMe to DCE (See Fig. 2 and Table 1). This shift indicated the formation of larger dipole moments in the emitting excited state. This behavior can be associated to the presence of *p*-vinylene group in the dendrimers molecular structures [6,7], where a charge-transfer character take place in the excited state formed after the light absorption process.

3.3. Dendrimers electrochemical characterization and polymeric films electrodeposition

The cyclic voltammograms corresponding to **D1** (Fig. 1) that holds only two branches, shows three clear oxidation process (See Fig. 3aI) with potential peak at 0.41, 0.82 and 1.19 V, whereas in the reversed potential sweep, the complementary reduction waves are not well defined. It has been established that the TPA centers hold oxidation potential lower than the related CBZ groups [26,33]. Therefore, the first oxidation wave can be assigned to the TPA radical cation generation, while, the second and third peaks are originated by the oxidation of the peripheral CBZ. The existence of two waves with different potential assigned to the CBZ oxidation could be ascribe to electrostatic interactions between the two adjacent charges [34]. The assignation of first oxidation process to the TPA radical cation generation is corroborated by the fact that when the applied potential is repetitive cycled until the first oxidation peak no current increment is observed. On the contrary, when the potential is cycled until the second and/or third peaks, a continuous current growing is clearly manifested (See Fig. 3aII) due to the coupling of CBZ radical cations, which drives to the formation of an electroactive film over the electrode surface [6,21]. This homogenous reaction processes is not possible when only the TPA center is oxidized, because the fact that their reactive cites are blocked [21,26,35]. On the other hand, when the CBZ groups are oxidized in successive sweeps, the voltammograms profile are keep similar, but a marked increase in the current density is observed, which would indicate the generation of an electroactive film on the Pt electrode surface. After 10 cycles of growing, the working Pt electrode was removed from the cell, rinsed and immersed in a monomer-free electrolytic solution. The electrochemical response of the film can be seen in Fig. 3aIII. The electrodeposited polymer film shows well-defined bell shaped oxidation and reduction peaks at ∼1.00 V, which is the typical CV current-potential behavior of immobilized redox centers [17,22,26,36,37].

Furthermore, the electrochemical behavior of the tri-branched macromolecules **D2** and **D3** (Fig. 1) is similar to the observed for **D1** (Fig. 3bI-III and cI-III). In addition, the TPA group located at the center of D3 seems not to affect the voltammogram profiles, but this dendrimer exhibits the lowest oxidation potential, indicating that the TPA core helps to stabilize the radical cation. This observation indicates that the different arrange of the dendrimer's branches in the space has negligible effect on the electrochemical behavior. On the other hand, another common feature observed in the three dendrimers redox behavior is the irreversible cathodic waves in the range of −0.2 V to −1.5 V, which are produced in the back sweep potential after dendrimeric materials oxidation. These reduction process are observed in both, the presence and absence of the monomers in solution (see the cyclic voltammograms shown in Fig. 3). The occurrence of this redox processes upon oxidation TPA and CBZ centers has been analyzed in detail by O. Yurchenko et al. [38] and were assigned to the reduction of oxidized σ-dimers formed after the oxidation of the aryl-amine centers. However, this oxidized σ-dimers are reduced in the back sweep at highly negative potentials (−0.5 to −1.5 V), and quickly decompose into the neutral starting species. In the electrodeposited **D1**, **D2** and **D3** polymeric films, it is expected that the high local concentration of reactive centers can induce the formation of σ-dimers. Therefore, the three compounds produce stable and reproducible electroactive films that remain on the electrode surface with an onset oxidation potential around 0.35 V ($E^{\#}_{\text{Film}}$). The energy values corresponding to the Highest Occupied Molecular Orbital (HOMO) and Lowest Unoccupied Molecular Orbital (LUMO) levels of the polymers were estimated (see Table 1). The position of the LUMO-HOMO in the absolute energy scale are in the range expected for phenylamine materials, commonly used as hole transporter layer [39], indicating that the electrodeposited dendrimeric films are suitable for their application in the construction of optoelectronic devices. However, the film morphology and topographic characteristics could be affected by the dendrimer structural and geometrical features [7]. The scanning electron microscopy (SEM) of the obtained polymer films on ITO electrode surface are shown in Fig. 4. In all cases the polymer structure completely covers the electrode, without cracks, pinholes or leaving unfilled spaces. However, the images show the presence of granulated surfaces, that in the case of **D1** polymeric film exhibits a more homogenous fashion than those obtained for other two dendrimers. **D3** forms the most inhomogeneous surface, which could be due to the presence of TPA electroactive core. Our group has re-

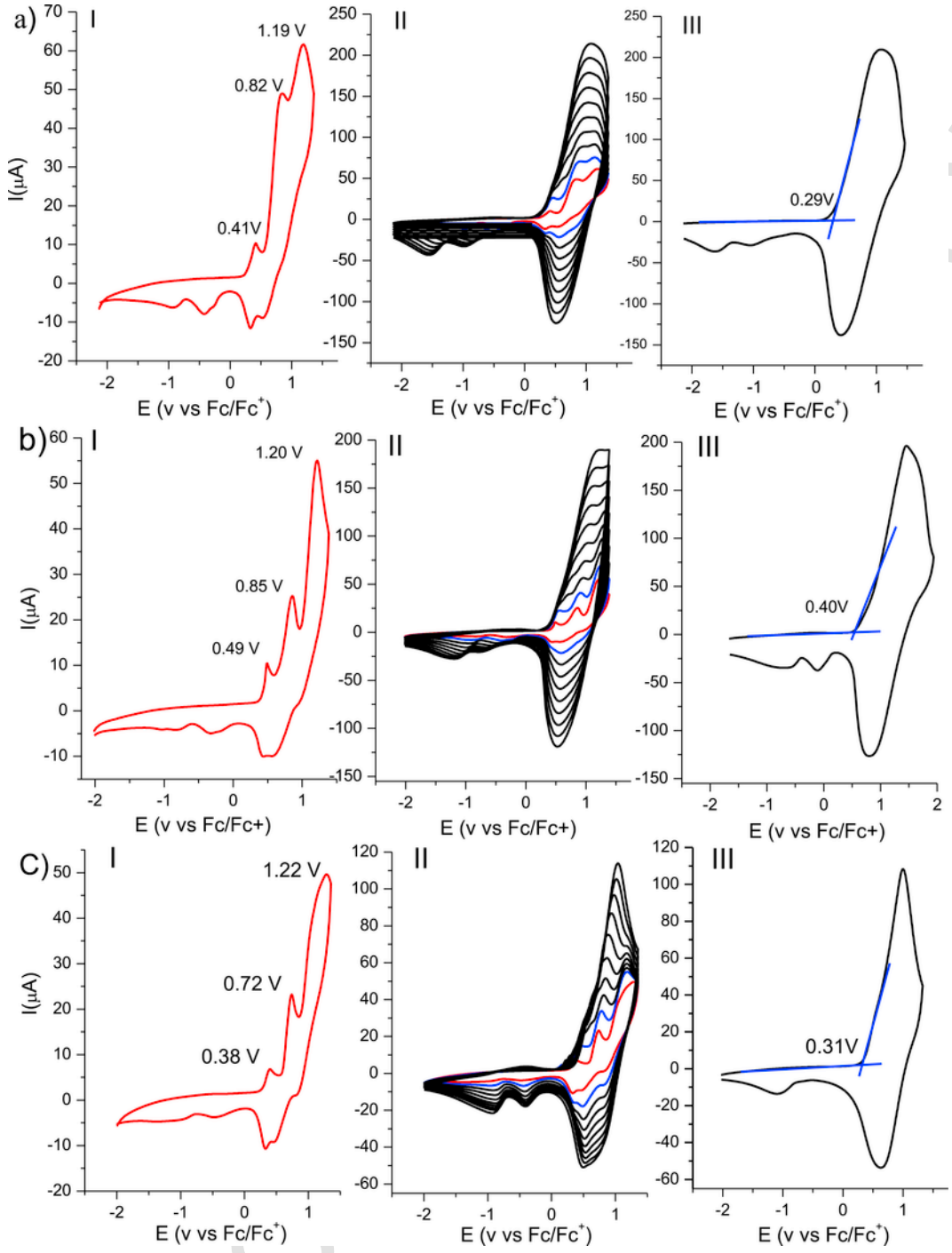

Fig. 3. Cyclic voltammograms of monomers and polymers of (a) **D1**. (b) **D2** and (c) **D3**. I) First voltammetry cycle (red) II) First (red), second (blue) and subsequent (black) voltammetry cycles. III) Cyclic voltammograms of the film deposited on Pt. Conditions: DCE with 0.1 M of TBAHPP, v = 0.075 V/s. (For interpretation of the references to color in this figure legend, the reader is referred to the Web version of this article.)

ported its effect on the dendrimer film morphology where surface irregularities were associated to the presence of the charged core [6,7].

On the other hand, the dendrimer structures also affect the film growing process. Under identical experimental conditions (monomer concentration, solvent, temperature, supporting electrolyte, scan program and rate) the formed films remarkably differ in their thicknesses. The electrodeposition of the three related macromolecules after ten growing cycles (according to Fig. 3) yields film thicknesses of 180, 210 and 363 nm for **D3**, **D1** and **D2**, respectively (Table 1). This effect could be originated by multiple reasons, including the kinetic of the film formation (altered by the molecular structure geometry), the electrodeposition efficiency and/or film density. Through the electrochemical and spectroelectrochemical analysis (see below), it was possible to demonstrate that the TPA nucleus of **D3** is oxidized during the electrodeposition process. This positive charge, placed at the central core of **D3**, produce coulombic repulsions between

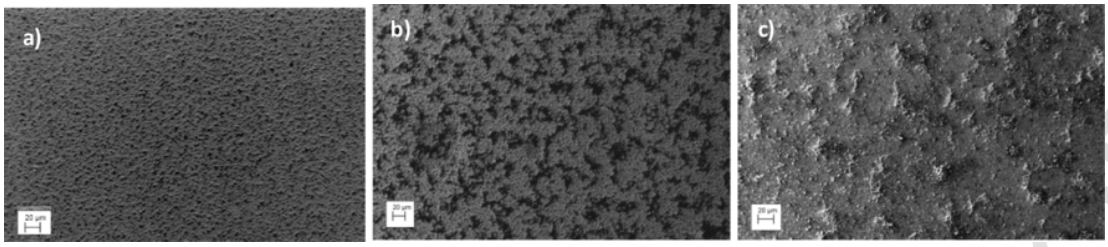

Fig. 4. Scanning electron microscopy of polymers films obtained from dendrimers (a) **D1**, (b) **D2**, (c) **D3**.

branches, which have influence in the film nucleation and growing processes, affecting its surface morphology [6,7].

3.4. Spectroelectrochemical characterization of the electrogenerated films

Spectroelectrochemical studies were carried out with electrodeposited dendrimeric polymers on semitransparent ITO electrodes. The electrodeposition conditions were described in Fig. 3. The films' absorption spectra of the three studied compounds were obtained in an applied potential range between 0 and 1.2 V (Fig. 5a-cI), which is the electrochemical window where the film redox processes occur (See films' voltammograms in Fig. 3). The films in their neutral state (bellow the oxidation onset potential, see Table 1) are semitransparent, exhibiting a large UV-light absorption (characteristics of the bis-carbazole π-π* transitions) [21,37]. The spectra also show tails that extend to the visible region, which give a pale-yellow coloration to the films. When the applied potentials are biased to positive voltages, and reach the films oxidation onset, the intensity of the electronic transitions at ~330 nm decrease, while new broad band appear between 400 and 1000 nm. These conditions produce a color change from pale-yellow to blue on the electrode that could be easily observed by the naked eye (See the electrode photographs in Fig. 5a-cI). This behavior can be analyzed considering the spectroscopic properties expected for the electrogenerated species in the dendrimeric polymeric films. It is known that TPA radical cations have an electronic transition around 650 nm, and bis-carbazole radical cations show two electronic transitions at 435 nm and 1030 nm approximately. These near IR region absorption band has been assigned to an intervalence charge-transfer between states in which the positive charge is centered at the different amino groups (bis-carbazole) [21], meanwhile, bis-carbazole dications absorb light at 722 nm [38,40]. All these charged species are possible to be electrogenerated under oxidation of the dendrimeric polymer films. Hence, all the observed spectral changes shown in Fig. 5a-cI are in agreement with the generation, upon film oxidation, of TPA radical cations and CBZ dimers cation and dication.

Analyzing the spectroelectrochemical behavior in more detail, it is clear for **D2** (see Fig. 5bI) at the first oxidation stages (until 1 V applied potential) the development of a band at ~650 nm, due to the absorption of the electrogenerated TPA radical cations. At more anodic applied potential, this band is further hidden because the apparition of the bis-carbazole dication light absorption band centered at ~750 nm. In addition, it is evident the formation and vanishing of the band as-

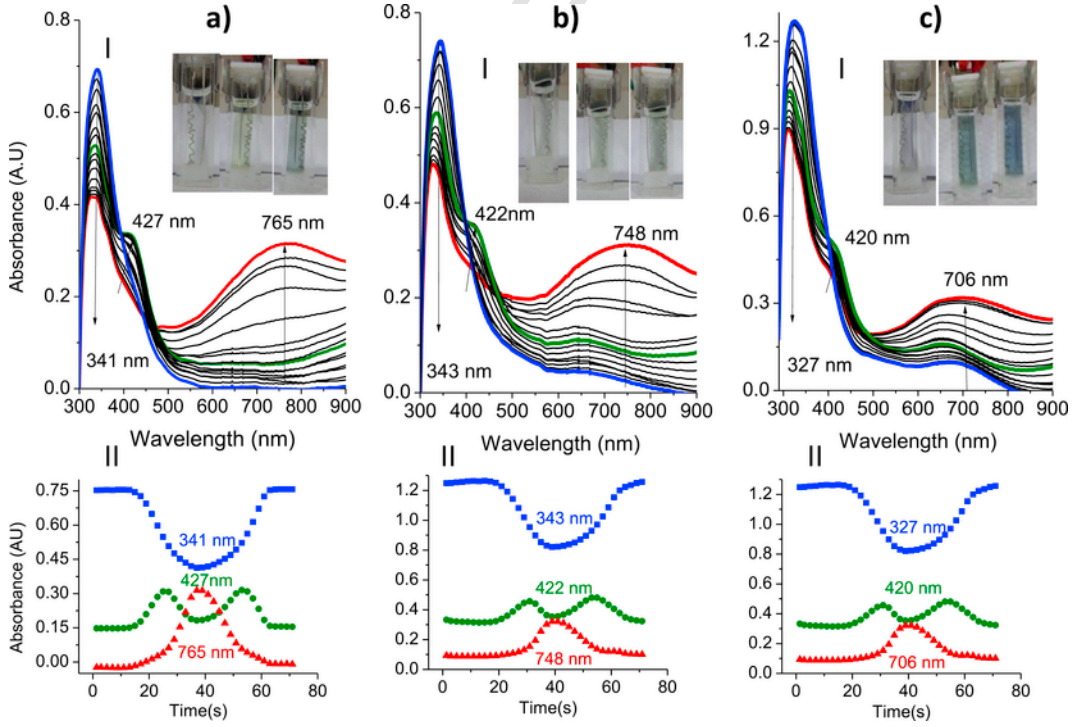

Fig. 5. Spectroelectrochemistry of electrodeposited thin films on ITO electrodes at different applied potentials of: (a) **D1**, (b) **D2** and (c) **D3**. I) Spectroelectrograms. The photographs show the electrodes color at different redox states. II) Absorbance transients at selected wavelengths.

sociated to the bis-carbazole radical cations at ~420 nm. These depicted spectral changes are also observed for the other two dendrimeric films (**D1** and **D3**), as it is shown in Fig. 5a-cI. Thus, the spectroscopy analysis supports the electrodeposition of the dendrimers through the electro-initiated coupling of peripheral CBZ radial cations and consequently, the generated CBZ-CBZ electroactive centers work as cross-linkers in the dendrimeric film molecular structures.

On the other hand, in the case of **D3**, the appearance of a band assigned to TPA radical cation (~650 nm) is detected, even at potential values where its formation it is not expected (See Fig. 5cI). This result agrees with the already observed spectra features for related structures [7], where a positive charge remained trapped or isolated in the TPA dendrimer core. Fig. 5a-cII show the absorbance transients corresponding to the main absorption changes, observed during the oxidation/reduction cycles applied to the electrodes in the spectroelectrochemistry analysis (See the arrows in Fig. 5a-cI). As the applied potential changes, it can be clearly seen that all traces in the near IR region reach a maximum when the film is fully oxidized, and they decrease when the potential scan is inverted, denoting the generation and reduction of the bis-carbazole dications. While, the traces at around 425 nm denote the formation of bis-carbazole radical cation in the forward and reverse scan. Finally, the traces in the UV region assigned to bis-carbazole π-π* transitions decreases as the films are oxidized and they are fully recovered at the end of the voltammograms. Thus after the reverse scan, all the traces reached the starting light absorption values, which indicates that the dendrimeric films undergoes fully reversible redox processes, highlighting the chemical stability of the generated charged species.

3.5. Hole mobility

Charge carrier mobility is a key material parameter in optoelectronic devices performance [39]. Among tested organic materials, some arylamines derivatives, exhibiting hole mobility exceeding $10^{-3}\,cm^2\,V^{-1}\,s^{-1}$, have been widely used as HTM in optoelectronic applications like organic light emitting diodes (OLEDs) [41,42]. The molecular structural parameters can influence the hole transport materials properties, for example in spiro conformation or dendrimer shape [43,44]; moreover, the film deposition method can affect the charge mobility [45,46]. Therefore, the assessment of the hole transport properties of the dendrimeric electrodeposited films, can provide crucial understanding regarding the relationship between molecular structures and hole mobility. The dendrimers charge mobility can be determinate by analyzing the current-voltage curves of the hole-only devices using the space-charge-limited current (SCLC) theory [3,47]. This model predicts that the current behavior at low range of applied potential, considering that the electric field has no relevant contribution, respond to the relationship outline in Eq. (1):

$$J_{SCL} = \frac{9}{8}\,\varepsilon\mu_p\,\frac{V^2}{d^3} \qquad (1)$$

where J is the current density, $\varepsilon=\varepsilon_0\varepsilon_r$ permittivity of the polymer, d the dendrimer films thickness and the μ_p the hole mobility. In Fig. 6 are shown the experimental J-V curves of hole-only devices built by electrodeposition method. The studied devices consist of a single electrodeposited dendrimeric polymer layer, which is sandwiched between two electrodes with the following configuration: ITO/den-

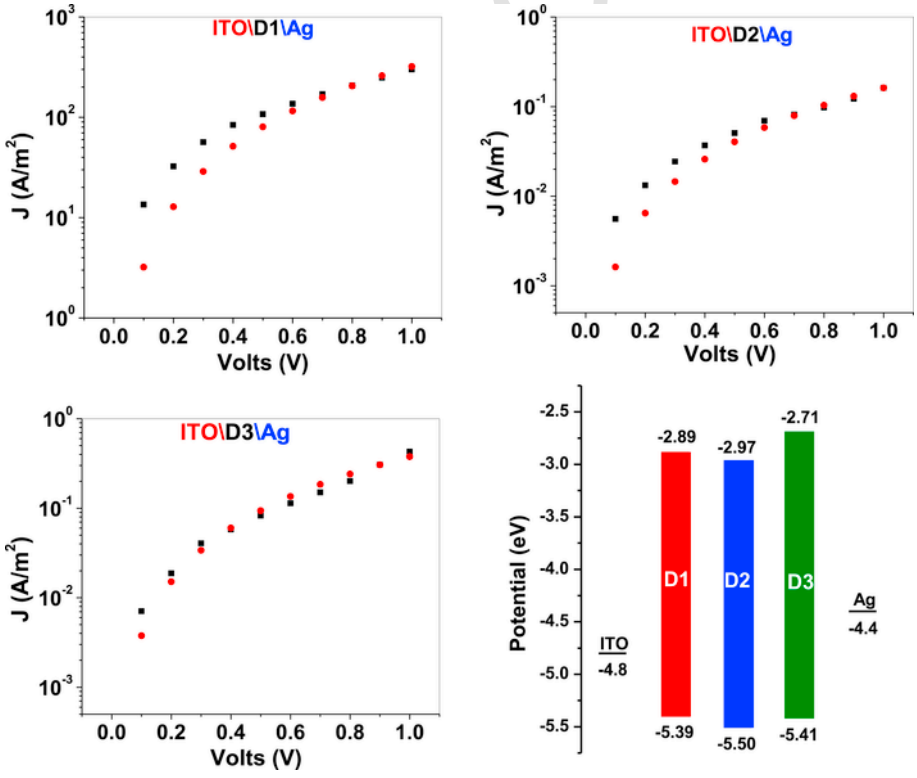

Fig. 6. Current density (■) vs. applied potential measured curves at room temperature of ITO/dendrimer films/Ag single layer devices. Calculated J-V values (●) from SCLC model (Eq. (1)). Film thickness: **D1** 191 nm, **D2** 394 nm and **D3** 169 nm.

drimers/Ag. The ITO electrode is used as a hole injector, while on the top of the dendrimer polymer layer Ag contact was evaporated as hole collector. Both contacts work functions are close to the HOMO of the dendrimeric materials, preventing electron injection from the negatively biased electrode (See picture inset in Fig. 6).

The dendrimers film hole mobility were calculated fitting the J-V experimental curves with SCLC model (Eq. (1)) using a dielectric constant $\varepsilon = 3$, in agreement with the reported for close related HTMs [48]. The results obtained are shown in Fig. 6a–c μ_p values of 7.30 10^{-7} cm^2/V, and 7.30 10^{-6} cm^2/V were obtained for **D3** and **D2**, respectively; while for **D1** yielded a noticeable higher hole mobility value of 8.98 10^{-4} cm^2/V. These dendrimeric films hole mobility are in the range to those reported for the well-known TPA derivatives films, deposited by other methods [41,42]. The carrier transport model in an amorphous organic solid is generally described as charge carriers hopping along the channels between localized hopping sites [49]. This mechanism strongly dependents on the intermolecular distance and the interaction degree between adjacent hopping sites. Among the studied molecular structures, **D1** exhibits the highest hole mobility, which can be associated to a less spatially hindering moieties that allow intermolecular interactions. In despite of the fact that **D2** and **D3** dendrimeric monomers hold more branched structures, the tridimensional polymeric network formed by electropolymerization of **D1** monomer allows the higher hole mobility. It has been shown that the dendrimer size and peripheral groups are key parameters for the dendrimeric films charge mobility, because these structural properties can affect the charge transfer rates between neighboring dendrimer molecules throughout an insulating effect [43]. As it is shown in Fig. 4, **D1**, which holds the highest charge mobility, produces films with surface morphologies clearly different from the other two dendrimeric structures. As has been established [47], molecular assemblies with large coupling between adjacent units generated organic material with high charge mobility. Thus, it is possible that, upon electropolymerization, **D1** may generates an interdigitate structure with closely packed polymer chains, which furnishes a material with enhanced mobility. Such close packing also produces smooth morphology in the film surface, which is clearly observed in Fig. 4. However, the effect of charge trapping sites in the polymeric structure also can affect the carrier mobility in the dendrimeric films [47]. In the case of **D3** film, which has the lowest charge mobility, the spectroelectrochemical shows that the TPA radical cation remains trapped or isolated in the dendrimer core (see Fig. 5cI), showing that the TPA core can acts as efficient traps sites for hopping hole carries.

4. Conclusion

We were able to design and synthetize structurally related π-conjugated star-shape dendrimeric structures with electroactive end-groups. A convergent synthetic method was use to connect the branches to the dendrimer cores through a C—C Sonogashira-type coupling. The overall synthethic procedure gives good yields of each intermediates and final compounds. The electropolymerization makes possible the formation of dendrimeric conducting films over metallic and ITO electrodes, which hold interesting features, as reversible electrochemical processes, electrochromic effects and good hole mobility. All these physicochemical properties were related with the molecular structural characteristic of the dendrimers. All dendrimers shows similar electrochemical and spectroelectrochemical response, according with the presence of TPA-CBZ residues in their structures. However, **D1** polymer exhibits a hole mobility near two order of magnitude higher than the other dendrimers demonstrating that this parameter strongly dependent of the geometry of the molecular structure. In summary, the synthesis and electrodeposition procedures afforded materials that can be applied in development of electronic and/or optoelectronics devices.

Appendix A. Supplementary data

Supplementary data related to this article can be found at https://doi.org/10.1016/j.electacta.2017.12.137.

References

[1] B. Lüssem, C.M. Keum, D. Kasemann, B. Naab, Z. Bao, K. Leo, Doped organic transistors, Chem. Rev. 116 (2016) 13714–13751.
[2] P. Cheng, X. Zhan, Stability of organic solar cells: challenges and strategies, Chem. Soc. Rev. 45 (2016) 2544–2582.
[3] B. Geffroy, P. le Roy, C. Prat, Organic light-emitting diode (OLED) technology: materials, devices and display technologies, Polym. Int. 55 (2006) 572–582.
[4] R.J. Mortimer, D.R. Rosseinsky, P.M.S. Monk, Electrochromic materials and devices, Electrochromic Mater. Dev. 77 (2015) 1–638.
[5] O. Ostroverkhova, Organic optoelectronic materials: mechanisms and applications, Chem. Rev. 116 (2016) 13279–13412.
[6] M.I. Mangione, R.A. Spanevello, D. Minudri, D. Heredia, L. Fernandez, L. Otero, F. Fungo, Electropolymerization of functionalizaed carbazole end-capped dendrimers. Formation of conductive films, Electrochim. Acta 207 (2016) 143–151.
[7] M.I. Mangione, R.A. Spanevello, A. Rumbero, D. Heredia, G. Marzari, L. Fernandez, L. Otero, F. Fungo, Electrogenerated conductive polymers from triphenylamine end- capped dendrimers, Macromolecules 46 (2013) 4754–4763.
[8] K.T. Won, L. Yu-Hsien, H.H. Wu, F. Fungo, Synthesis and properties of dumbbell-shaped dendrimers containing 9-phenylcarbazole dendrons, Org. Lett. 9 (2007) 4531–4534.
[9] K. Albrecht, R. Pernites, M.J. Felipe, R.C. Advincula, K. Yamamoto, Patterning carbazole − phenylazomethine dendrimer films, Macromolecules 45 (2012) 1288–1295.
[10] W. Gao, J. Wang, Y. Lin, Q. Luo, Y. Ma, J. Dou, H. Tan, C.Q. Ma, Z. Cui, Functionalization of diketopyrrolopyrrole with dendritic oligothiophenes: synthesis, photophysical properties, and application in solar cells, J. Photochem. Photobiol. Chem. (2017).
[11] M. Auer-Berger, R. Trattnig, T. Qin, R. Schlesinger, M.V. Nardi, G. Ligorio, C. Christodoulou, N. Koch, M. Baumgarten, K. Müllen, E.J.W. List-Kratochvil, All-solution-processed multilayer polymer/dendrimer light emitting diodes, Org. Electron. Phys. Mater. Appl. 35 (2016) 164–170.
[12] Z. Zhong, S. Zhao, J. Pei, J. Wang, L. Ying, J. Peng, Y. Cao, An alkane-soluble dendrimer as electron-transport layer in polymer light-emitting diodes, ACS Appl. Mater. Interfac. 8 (2016) 20237–20242.
[13] M. Thelakkat, Star-shaped, dendrimeric and polymeric triarylamines as photoconductors and hole transport materials for electro-optical applications, Macromol. Mater. Eng. 287 (2002) 442–461.
[14] C. Adachi, K. Nagai, N. Tamoto, Molecular design of hole transport materials for obtaining high durability in organic electroluminescent diodes, Appl. Phys. Lett. 66 (1995) 2679.
[15] C. Adachi, T. Tsutsui, S. Saito, Blue light-emitting organic electroluminescent devices, Appl. Phys. Lett. 56 (1990) 799–801.
[16] I.R. de Moraes, S. Scholz, M. Hermenau, M.L. Tietze, T. Schwab, S. Hofmann, M.C. Gather, K. Leo, Impact of temperature on the efficiency of organic light emitting diodes, Org. Electron. 26 (2015) 158–163.
[17] M. Li, S. Tang, F. Shen, M. Liu, W. Xie, H. Xia, L. Liu, L. Tian, Z. Xie, F. Lu, M. Hanif, D. Lu, G. Cheng, Y. Ma, Electrochemically deposited organic luminescent films: the effects of deposition parameters on morphologies and luminescent efficiency of films, J. Phys. Chem. B 110 (2006) 17784–17789.
[18] Y. Yang, K. Mielczarek, A. Zakhidov, W. Hu, Efficient low bandgap polymer solar cell with ordered heterojunction de fi ned by nanoimprint lithography, ACS Appl. Mater. Interfac. 6 (2014) 19282–19287.
[19] F.C. Krebs, Fabrication and processing of polymer solar cells: a review of printing and coating techniques, Sol. Energy Mater. Sol. Cell. 93 (2009) 394–412.
[20] M. Gervaldo, M. Funes, J. Durantini, L. Fernandez, F. Fungo, L. Otero, Electrochemical polymerization of palladium (II) and free base 5,10,15,20-tetrakis(4-N,N-diphenylaminophenyl)porphyrins: its applications as electrochromic and photoelectric materials, Electrochim. Acta 55 (2010) 1948–1957.
[21] S. Hsiao, J. Hsueh, Electrochemical synthesis and electrochromic properties of new conjugated polycarbazoles from di (carbazol-9-yl) -substituted triphenylamine and N -phenylcarbazole derivatives, JEAC 758 (2015) 100–110.
[22] D. Heredia, L. Fernandez, L. Otero, M. Ichikawa, C. Lin, Y. Liao, S. Wang, K. Wong, F. Fungo, Electrochemical tuning of morphological and optoelectronic characteristics of donor-acceptor spiro-fluorene polymer film. Application in the building of an electroluminescent device, J. Phys. Chem. C 115 (2011) 21907–21914.

[23] P. Zabel, T. Dittrich, Y.L. Liao, C.Y. Lin, K.T. Wong, F. Fungo, L. Fernandez, L. Otero, Engineering of gold surface work function by electrodeposition of spirobifluorene donor-acceptor bipolar systems, Org. Electron. Physics, Mater. Appl. 10 (2009) 1307–1313.
[24] L. Otero, L. Sereno, F. Fungo, Y. Liao, C. Lin, Synthesis and properties of a novel electrochromic polymer obtained from the electropolymerization of a 9, 9 ' -spirobifluorene-Bridged donor - acceptor (D - a) bichromophore system, Chem. Mater. 18 (2006) 3495–3502.
[25] X. Cui, D.C. Martin, Electrochemical deposition and characterization of poly(3,4-ethylenedioxythiophene) on neural microelectrode arrays, Sensor. Actuator. B Chem. 89 (2003) 92–102.
[26] P. Rajakumar, A. Thirunarayanan, S. Raja, S. Ganesan, P. Maruthamuthu, Photophysical properties and dye-sensitized solar cell studies on thiadiazole-triazole-chalcone dendrimers, Tetrahedron Lett. 53 (2012) 1139–1143.
[27] M. Yu, S. Wang, S. Shao, J. Ding, L. Wang, X. Jing, F. Wang, Starburst 4,4′,4″-tris(carbazol-9-yl)-triphenylamine-based deep-blue fluorescent emitters with tunable oligophenyl length for solution-processed undoped organic light-emitting diodes, J. Mater. Chem. C 3 (2015) 861–869.
[28] Y.-S. Tsai, L.-A. Hong, F.-S. Juang, C.-Y. Cheng, D.-G. Wang, Using double-layer host emitter structure to manufacture blue and white phosphorescent organic light emitting diodes, J. Nanosci. Nanotechnol. 16 (2016) 11750–11756.
[29] H. Nonami, S. Fukui, R. Erra-Balsells, β-Carboline alkaloids as matrices for matrix-assisted ultraviolet laser desorption time-of-flight mass spectrometry of proteins and sulfated oligosaccharides: a comparative study using phenylcarbonyl compounds, carbazoles and classical matrices, J. Mass Spectrom. 32 (1997) 287–296.
[30] C.M. Cardona, W. Li, A.E. Kaifer, D. Stockdale, G.C. Bazan, Electrochemical considerations for determining absolute frontier orbital energy levels of conjugated polymers for solar cell applications, Adv. Mater. 23 (2011) 2367–2371.
[31] C. Glaser, Beiträge zur kenntniss des acetenylbenzols, Chem. Ber. 2 (1869) 422–424.
[32] A. Tomkeviciene, J.V. Grazulevicius, K. Kazlauskas, A. Gruodis, S. Jursenas, T.H. Ke, C.C. Wu, Impact of linking topology on the properties of carbazole trimers and dimers, J. Phys. Chem. C 115 (2011) 4887–4897.
[33] J. Natera, L. Otero, L. Sereno, F. Fungo, N. Sen Wang, Y.M. Tsai, T.Y. Hwu, K.T. Wong, A novel electrochromic polymer synthesized through electropolymerization of a new donor-acceptor bipolar system, Macromolecules 40 (2007) 4456–4463.
[34] A.J. Bard, L.R. Faulkner (Eds.), Electrochemical Methods Fundamentals and Applications,, John Wiley & Sons, Inc, New York, 1944.
[35] J. Lu, P.F. Xia, P.K. Lo, Y. Tao, M.S. Wong, Synthesis and properties of multi-triarylamine-substituted carbazole-based dendrimers with an oligothiophene core for potential applications in organic solar cells and light-emitting diodes, Chem. Mater. 18 (2006) 6194–6203.
[36] D. Heredia, J. Natera, M. Gervaldo, L. Otero, F. Fungo, C.Y. Lin, K.T. Wong, Spirobifluorene-bridged donor/acceptor dye for organic dye-sensitized solar cells, Org. Lett. 12 (2010) 12–15.
[37] J. Natera, L. Otero, F. D'Eramo, L. Sereno, F. Fungo, N. Sen Wang, Y.M. Tsai, K.T. Wong, Synthesis and properties of a novel cross-linked electroactive polymer formed from a bipolar starburst monomer, Macromolecules 42 (2009) 626–635.
[38] O. Yurchenko, D. Freytag, L. Borg, R. Zentel, Jürgen Heinze, S. Ludwigs, Electrochemically induced reversible and irreversible coupling of triarylamines, J. Phys. Chem. B 116 (2012) 30–39.
[39] Y. Shirota, H. Kageyama, Charge carrier transporting molecular materials and their applications in devices charge carrier transporting molecular materials and their applications in devices, Chem. Rev. 107 (2007) 953–1010.
[40] S.K. Chiu, Y.C. Chung, G.S. Liou, Y.O. Su, Electrochemical and spectral characterizations of 9-phenylcarbazoles, J. Chin. Chem. Soc. 59 (2012) 331–337.
[41] P. Strohriegl, J.V. Grazulevicius, Charge-transporting molecular glasses, Adv. Mater. 14 (2002) 1439–1452.
[42] H.H. Fong, K.C. Lun, S.K. So, Hole transports in molecularly doped triphenylamine derivative, Chem. Phys. Lett. 353 (2002) 407–413.
[43] A.J. Mozer, C.Q. Ma, W.W.H. Wong, D.J. Jones, P. Bäuerle, G.G. Wallace, The effect of molecule size and shape on free charge generation, transport and recombination in all-thiophene dendrimer:fullerene bulk heterojunctions, Org. Electron. Physics, Mater. Appl. 11 (2010) 573–582.
[44] J. Lupton, I. Samuel, R. Beavington, M. Frampton, P. Burn, H. Bässler, Control of mobility in molecular organic semiconductors by dendrimer generation, Phys. Rev. B 63 (2001), 155206.
[45] H. Yan, Z. Chen, Y. Zheng, C. Newman, J.R. Quinn, F. Dötz, M. Kastler, A. Facchetti, A high-mobility electron-transporting polymer for printed transistors, Nature 457 (2009) 679–686.
[46] C.D. Dimitrakopoulos, D.J. Mascaro, Organic thin-film transistors: a review of recent advances, IBM J. Res. Dev. 45 (2001) 11–27.
[47] H. Bässler, A. Köhler, Charge Carrier Mobility in Amorphous Organic Semiconductors, Woodhead Publishing Limited, 2013.
[48] Z.B. Wang, M.G. Helander, M.T. Greiner, J. Qiu, Z.H. Lu, Carrier mobility of organic semiconductors based on current-voltage characteristics, J. Appl. Phys. 107 (2010) 2–5.
[49] R.A. Marcus, Electron transfer reactions in chemistry: theory and experiment (nobel lecture), Angew. Chem. Int. Ed. 32 (1993) 1111–1121.